Striction-Coupled Magnetoresistance in Perovskite-Type Manganese Oxides

H. Kuwahara, Y. Tomioka, Y. Moritomo,* A. Asamitsu, M. Kasai, R. Kumai, Y. Tokura†

Magnetoresistance resulting in a drop in resistivity of more than three orders of magnitude that is strongly coupled to lattice striction has been observed under a relatively low magnetic field (0.4 tesla at 115 kelvin) for a single crystal of perovskite-type manganese oxide with finely controlled ionic radii of the A sites, $(Nd,Sm)_{1/2}Sr_{1/2}MnO_3$. The colossal magnetoresistance phenomena are viewed as a first-order insulator-to-metal phase transition induced by a magnetic field, which accompanies a metamagnetic (antiferromagnetic-to-ferromagnetic) transition and a structural change in the lattice. Clear hystereses and abrupt changes in magnetization, striction, and resistivity were observed in increasing and decreasing magnetic fields at temperatures (113 to 150 kelvin) just above the Curie temperature.

Giant magnetoresistance (MR), a large change in electrical resistance in response to an external magnetic field, has been extensively studied in two kinds of materials: thin films of metallic multilayers (*1*, *2*) and perovskite-type carrier-doped manganese oxides (*3*–*6*). The latter have attracted interest recently for their colossal MR value even though they require higher magnetic fields than the former system. For applications such as sensors, MR reading heads, and MR random access memories, materials need not only a large MR value but also a low driving (saturation) field. From this viewpoint, we have systematically explored single crystals of the perovskite-type manganese oxides and found that the compounds $(Nd_{1-y}Sm_y)_{1/2}Sr_{1/2}MnO_3$ with a particular composition ($0.5 \leq y \leq 0.95$) show colossal MR arising from the coupling with lattice striction under a low magnetic field that can be generated by a permanent magnet. Here we describe the striction-coupled MR phenomena with a character of the first-order phase transition, as investigated by measurements of magnetization (M), striction ($\Delta L/L$, where ΔL is the change in crystal length L, which is related to changes in crystallographic lattice parameters), and resistivity (ρ) for thermal and magnetic-field scans.

The system investigated here, $(Nd,Sm)_{1/2}Sr_{1/2}MnO_3$, is derived by decreasing the tolerance factor [or, equivalently, the one-electron band width (*7*)] of $Nd_{1-x}Sr_xMnO_3$ ($x = 1/2$), which undergoes a phase transition from a ferromagnetic metallic state to a charge-ordered insulating antiferromagnetic state at 158 K (*8*). We finely controlled the tolerance factor with the use of a solid solution (Nd,Sm) on the perovskite A sites while keeping the nominal hole concentration x at a commensurate value ($x = 1/2$). The crystal of $(Nd_{1-y}Sm_y)_{1/2}Sr_{1/2}MnO_3$ ($y = 0.938$) and a dozen related crystals ($y = 0$ to 0.95) were grown by the floating zone method in a halogen-lamp image furnace. The Rietveld analysis of powder x-ray diffraction (XRD) data revealed that the sample is single phase without any other secondary or impurity phase. The structure of the $y = 0.938$ crystal at room temperature was determined to be orthorhombic (*Pbnm*, the so-called $GdFeO_3$ type; number of formula in the unit cell $Z = 4$) by a least-squares refinement of data collected with a four-circle XRD apparatus: cell constants are $a = 5.4376(8)$ Å, $b = 5.4226(8)$ Å, and $c = 7.6529(9)$ Å ($a \approx b \approx \sqrt{2}a_p$ and $c \approx 2a_p$, a_p being the unit cell length of the cubic perovskite; numbers in parentheses are standard errors in the last digit). Inductively coupled plasma mass spectrometry indicated stoichiometry $y = 0.938 \pm 0.002$.

Figure 1 shows the temperature (T) dependence of the inverse magnetization (H/M, where the applied magnetic field $H = 0.5$ T), ρ, and $\Delta L/L$ for the $y = 0.938$ crystal of $(Nd_{1-y}Sm_y)_{1/2}Sr_{1/2}MnO_3$. At the Curie temperature $T_c = 113$ K, ρ drops sharply by more than three orders of magnitude from a nonmetallic to a typically metallic value (5×10^{-4} ohm·cm). The inverse magnetization at T_c also dropped sharply, yielding $M = 3.5$ Bohr magnetons (μ_B) per Mn site, which corresponds to an almost fully spin-polarized state. Such a ferromagnetic metal state is caused by the so-called double-exchange interaction between the Mn^{3+} and Mn^{4+} ions, that is, ferromagnetic coupling between the local $3d$ (t_{2g} state) spins mediated by itinerant $3d$ electrons (e_g state) (*6*, *9*). The H/M versus T curve shows Curie-Weiss–like behavior above 300 K (dashed line in Fig. 1), but a clear deviation is evident with a slight upturn or plateau around 200 K down to T_c at 113 K. In accord with the beginning of the plateau in the H/M curve, the slope of the ρ curve becomes steeper with decreasing temperature and shows a deviation from the thermal-activation–type temperature dependence (with the activation energy of ≈480 K). In this temperature region (113 to ≈200 K), the ferromagnetic double-exchange interaction seems to be suppressed by localization of mobile carriers or an antiferromagnetic interaction, or both. This antiferromagnetic interaction may be relevant to a charge-ordering instability, the real-space ordering of doped holes, observed in similar manganese oxides (*8*, *10*, *11*) such as $Pr_{1/2}Ca_{1/2}MnO_3$ with the charge-ordering temperature of 240 K (*12*).

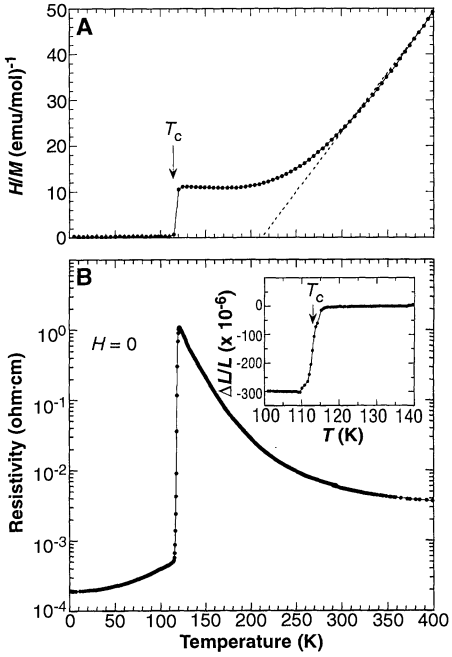

Fig. 1. Temperature dependence of (**A**) the inverse magnetization (measured at a magnetic field $H = 0.5$ T), (**B**) resistivity, and (**inset**) striction in a $(Nd_{1-y}Sm_y)_{1/2}Sr_{1/2}MnO_3$ ($y = 0.938$) crystal. The striction measurement was performed with use of a strain gauge attached to the crystal. The critical temperature T_c for the transition from the high-resistive (antiferromagnetic-like) state to the low-resistive ferromagnetic one with the magnetization of ≈3.5μ_B per Mn site is indicated. A Curie-Weiss law is shown in (A) by a dashed line. Upon phase transition, the resistivity abruptly changes by more than three orders of magnitude. Simultaneously, the crystal structure also undergoes a change, as evidenced by the striction data. Reflecting the nature of the first-order phase transition, each quantity shows hysteresis (see Fig. 2).

H. Kuwahara, Y. Tomioka, Y. Moritomo, A. Asamitsu, M. Kasai, R. Kumai, Joint Research Center for Atom Technology, Tsukuba 305, Japan.
Y. Tokura, Joint Research Center for Atom Technology, Tsukuba 305, and Department of Applied Physics, University of Tokyo, Tokyo 113, Japan.

*Present address: Center for Integrated Research in Science and Engineering, Nagoya University, Nagoya 464-01, Japan.
†To whom correspondence should be addressed.

In accord with these abrupt changes in electronic and magnetic properties, a structural change in the lattice occurs, which was confirmed by measurements of $\Delta L/L$ made with a uniaxial strain gauge (Kyowa Electric Instrument, Tokyo) attached to an arbitrary direction of the crystal (*13*); the striction was monitored by the gauge as a change in the resistance. The temperature-controlled XRD revealed that the space group of the crystal structure was unchanged, but the lattice parameters abruptly changed at T_c: both the *a* and *b* axes shrank by ≈0.14% and *c* expanded by ≈0.19% during a cooling run [hence, striction data (Fig. 1B) mainly reflected a certain direction in the *ab* plane]. These changes seem to arise from a relaxation of distortion inherent to charge-ordering instability, because similar changes are observed at the transition from a charge-ordered insulator to a ferromagnetic metal in $Nd_{1/2}Sr_{1/2}MnO_3$ (*8*) (in the case of $Nd_{1/2}Sr_{1/2}MnO_3$, the charge-ordered state collapses in the course of the warming run). In contrast to ordinary second-order ferromagnetic transitions for manganese oxides with double-exchange interaction, sharp changes in resistivity and magnetization are observed at T_c, which are believed to be results of the first-order phase transition. Thus, the ferromagnetic transition is strongly coupled to the lattice and charge degrees of freedom and accompanies the thermal hysteresis, reflecting the nature of the first-order phase transition (Fig. 2). Such a first-order–like ferromagnetic transition can be observed only in a limited range of the composition for $(Nd_{1-y}Sm_y)_{1/2}Sr_{1/2}MnO_3$: $0.5 \leq y \leq 0.95$.

The critical temperature for the transition of $(Nd_{1-y}Sm_y)_{1/2}Sr_{1/2}MnO_3$ (y = 0.938) to the ferromagnetic metal (Fig. 2) increases with magnetic field intensity. The thermal hysteresis narrows with magnetic field intensity (or with increase of the transition temperature) and disappears for $H > 2$ T or transition temperatures above about 150 K. As the transition temperature approaches ≈200 K [where the plateau of the *H*/*M* deviation from the Curie-Weiss law was observed (Fig. 1)] during application of a magnetic field of more than 4 T, the character of the phase transition gradually changes; that is, the drop in resistivity becomes gradual. This feature may be explained by the conventional lattice-irrelevant mechanism: the spin scattering is reduced by the field-induced alignment of the local spins, which is the case for $La_{1-x}Sr_xMnO_3$ (*6*).

To further clarify the character of the phase change, we investigated M, $\Delta L/L$, and ρ as a function of H at several fixed temperatures just above T_c (Fig. 3). In each case, we observed a clear hysteresis against the field scan, which is characteristic of the first-order phase transition. The resistivity changed by more than three orders of magnitude under a magnetic field of 0.4 T at 115 K, and hence, ρ appears to approach zero in a linear-scale plot (Fig. 3C).

The *M*-*H* curves (Fig. 3A) indicate that this transition is metamagnetic: antiferromagnetic-like branches are abruptly switched to the ferromagnetic ones at respective transition fields. The hysteretic field region becomes narrower as T increases from T_c (113 K) or as the transition magnetic field increases. The hysteretic field region disappears above about 150 K (corresponding to the transition field of 2 T), which is consistent with the case of the thermal scan (Fig. 2). As in the thermal scan, the characteristics of MR gradually change from behavior similar to a first-order transition to that of ordinary MR with increase of the transition field (or temperature); in the latter case, $\Delta\rho/\rho(0)$ {that is, $[\rho(0) - \rho(H)]/\rho(0)$} is proportional to $(M/M_s)^2$, as observed for $La_{1-x}Sr_xMnO_3$ (*6*, *14*) [$\rho(H)$ is the resistivity in magnetic field H, $\rho(0)$ is the resistivity in zero field, and M_s is the saturation magnetization (3.5 μ_B per Mn site)].

The change in ρ is accompanied by the lattice structural change. Magnetostriction ($\Delta L/L$) resulting from structural changes (measured by the strain gauge method) (Fig. 3B) causes the crystal to shrink abruptly by ≈0.025% at a critical magnetic field corresponding to the resistive and metamagnetic transitions. The magnetostriction also shows hysteresis below 150 K against changes in the magnetic field. The field-induced changes of M, $\Delta L/L$, and ρ are thus consistent with each other, and the colossal MR is ascribed to the first-order phase transition associated with simultaneous changes of the magnetic and lattice structures.

We compared the MR characteristics of the present manganites with other known representative MR materials (Fig. 4): a perovskite-type oxide of $La_{1-x}Sr_xMnO_3$ (x = 0.15) at just above its Curie temperature of 240 K (*6*) and an antiferromagnetically coupled Co/Cu superlattice at 4.2 K (*2*). The former compound is a prototype for the perovskite-type manganese oxide that shows a maximal MR around T_c: $\rho(H)/\rho(0)$ decreases to <0.1 at 15 T, but $\Delta\rho = \rho(0) - \rho(H)$ is proportional to the square of field intensity

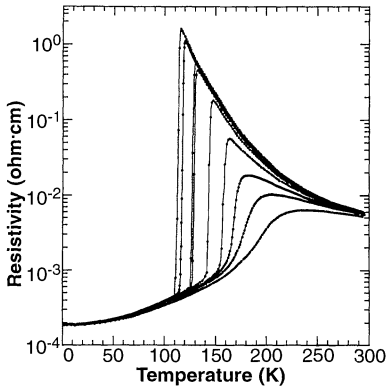

Fig. 2. Temperature dependence of resistivity under various magnetic fields for a $(Nd_{1-y}Sm_y)_{1/2}Sr_{1/2}MnO_3$ (y = 0.938) crystal. The gray region shows the thermal hysteresis, which gradually narrowed with increasing magnetic field intensities and disappeared above 2 T. The magnetic fields, for the upper set of curves to the lower set, were H = 0, 1, 2, 3, 4, 5, and 7 T. The transition temperature increased with magnetic field.

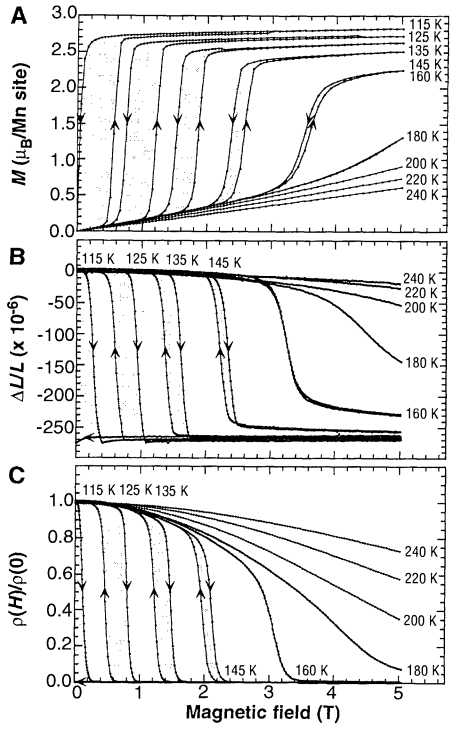

Fig. 3. (**A**) Magnetization, (**B**) striction, and (**C**) resistivity as a function of magnetic field in a $(Nd_{1-y}Sm_y)_{1/2}Sr_{1/2}MnO_3$ (y = 0.938) crystal at temperatures just above T_c. The gray areas indicate the hysteretic field region for each quantity.

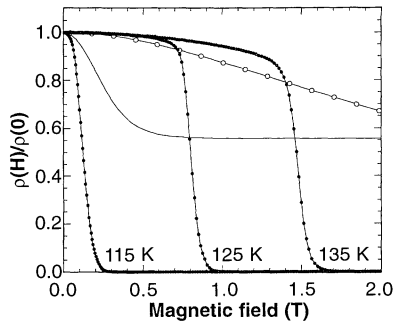

Fig. 4. Comparison of isothermal magnetoresistance for $(Nd_{1-y}Sm_y)_{1/2}Sr_{1/2}MnO_3$ (y = 0.938) (solid circles) to those for other typical giant-MR materials: (open circles) a perovskite-type oxide of $La_{1-x}Sr_xMnO_3$ (x = 0.15) at 254 K (near the Curie temperature of 240 K) (*6*) and (solid line with no symbols) an antiferromagnetically coupled Co/Cu superlattice at 4.2 K (*2*).

in such a low-field region. The latter system is, on the other hand, an example of the magnetic superlattice films that show characteristics much less dependent on T below room temperature. The single crystal of the $(Nd,Sm)_{1/2}Sr_{1/2}MnO_3$ is more sensitive to low magnetic fields than the other compounds and has the largest MR value among them (Fig. 4), although the temperature region is limited (see also Fig. 3C) compared with those of the magnetic superlattice systems. The observed MR value, defined as $\Delta\rho/\rho(H)$, of the $(Nd,Sm)_{1/2}Sr_{1/2}MnO_3$ compound reaches 10^4 percent at 115 K under a magnetic field of 0.25 T and 4×10^4 percent at 125 K and 1.0 T. A MR effect of similar magnitude has been attained for thin films of $La_{1-x}Ca_xMnO_3$ (*4*) and $Nd_{1-x}Sr_xMnO_3$ (*5*) and for single crystals of the perovskite-type manganese oxides such as $Pr_{1-x}Sr_xMnO_3$ ($x = 0.5$) (*10*), $Nd_{1-x}Sr_xMnO_3$ ($x = 0.5$) (*8*), and $Pr_{1-x}Ca_xMnO_3$ ($0.3 \leq x \leq 0.5$) (*12*). Nevertheless, the driving (saturation) magnetic field of $(Nd,Sm)_{1/2}Sr_{1/2}MnO_3$ is exceptionally low. The switching-like colossal MR accompanying the field hysteresis may have some potential for application to magnetoswitching materials and devices with memory function.

REFERENCES AND NOTES

1. M. N. Baibich *et al.*, *Phys. Rev. Lett.* **61**, 2472 (1988); S. S. P. Parkin, N. More, K. P. Roche, *ibid.* **64**, 2304 (1990).
2. S. S. P. Parkin, R. Bhadra, K. P. Roche, *ibid.* **66**, 2152 (1991).
3. R. M. Kusters, J. Singleton, D. A. Keen, R. McGreevy, W. Hayes, *Physica B* **155**, 362 (1989); K. Chahara, T. Ohno, M. Kasai, Y. Kozono, *Appl. Phys. Lett.* **63**, 1990 (1993); R. von Helmolt, J. Wecker, B. Holzapfel, L. Shultz, K. Samwer, *Phys. Rev. Lett.* **71**, 2331 (1993); Y. Tokura *et al.*, *J. Phys. Soc. Jpn.* **63**, 3931 (1994).
4. S. Jin *et al.*, *Science* **264**, 413 (1994); M. McCormack *et al.*, *Appl. Phys. Lett.* **64**, 3045 (1994).
5. G. C. Xiong *et al.*, *Appl. Phys. Lett.* **66**, 1427 (1995); G. C. Xiong, Q. Li, H. L. Ju, R. L. Greene, T. Venkatesan, *ibid.*, p. 1689.
6. A. Urushibara *et al.*, *Phys. Rev. B* **51**, 14103 (1995).
7. J. B. Torrance, P. Lacorre, A. I. Nazzal, E. J. Ansaldo, Ch. Nidermayer, *ibid.* **45**, 8209 (1992); H. Y. Hwang, S.-W. Cheong, P. G. Radaelli, M. Marezio, B. Batlogg, *Phys. Rev. Lett.* **75**, 914 (1995).
8. H. Kuwahara, Y. Tomioka, A. Asamitsu, Y. Moritomo, Y. Tokura, *Science* **270**, 961 (1995).
9. G. H. Jonker and J. H. Van Santen, *Physica* **16**, 337 (1950); P. W. Anderson and H. Hasegawa, *Phys. Rev.* **100**, 675 (1955); P.-G. de Gennes, *ibid.* **118**, 141 (1960).
10. Y. Tomioka, A. Asamitsu, Y. Moritomo, H. Kuwahara, Y. Tokura, *Phys. Rev. Lett.* **74**, 5108 (1995).
11. P. Shiffer, A. P. Ramirez, W. Bao, S.-W. Cheong, *ibid.* **75**, 3336 (1995).
12. Y. Tomioka, A. Asamitsu, Y. Moritomo, Y. Tokura, *J. Phys. Soc. Jpn.* **64**, 3626 (1995); Y. Tomioka, A. Asamitsu, H. Kuwahara, Y. Moritomo, Y. Tokura, *Phys. Rev. B* **53**, R1689 (1996).
13. A. Asamitsu, Y. Moritomo, Y. Tomioka, T. Arima, Y. Tokura, *Nature* **373**, 407 (1995).
14. N. Furukawa, *J. Phys. Soc. Jpn.* **63**, 3214 (1994).

15. We thank N. Nonose for the inductively coupled plasma measurements. Supported by the New Energy and Industrial Technology Development Organization (NEDO) of Japan.

6 November 1995; accepted 5 February 1996

Earliest Complete Dentition of an Anthropoid Primate from the Late Middle Eocene of Shanxi Province, China

K. Christopher Beard, Yongsheng Tong, Mary R. Dawson, Jingwen Wang, Xueshi Huang

The complete lower dentition of a new species of the basal anthropoid genus *Eosimias* shows a combination of primitive and derived traits unknown in other living or fossil primates. Although certain dental traits are decidedly more primitive in *Eosimias* than in other basal anthropoids, numerous derived aspects of jaw and dental morphology support the anthropoid affinities of Eosimiidae. Eosimiids document an early structural phase in the evolution of higher primates. Phylogenies that derive early anthropoids from cercamoniine adapiforms are inconsistent with eosimiid anatomy. Because early fossil anthropoids are known from both Asia and Africa, the fossil record is presently insufficient to specify the continent on which this clade originated.

The extinct primate family Eosimiidae was first described in 1994 on the basis of fossils collected from the middle Eocene Shanghuang fissure-fillings of southern Jiangsu Province, China (*1*). Although fossils documenting several species of Eosimiidae are known, only one of these, *Eosimias sinensis*, has been described to date. *Eosimias sinensis* was originally interpreted as a member of an early basal radiation of anthropoid or higher primates, the taxon that today includes New and Old World monkeys, apes, and humans. Subsequently, the phylogenetic hypothesis that *Eosimias* is a basal anthropoid has been widely criticized, and several workers have even doubted its primate affinities (*2–4*). Here we describe a new eosimiid species, *Eosimias centennicus* (*5*), on the basis of fossils collected during May 1995 fieldwork in the Eocene Heti Formation, Yuanqu Basin, southern Shanxi Province, China (Fig. 1). These new specimens include the first complete lower dentition of eosimiid primates ever found. The anatomical information yielded by these fossils confirms the anthropoid affinities of Eosimiidae, thus providing new data on temporal, biogeographic, and phylogenetic aspects of anthropoid origins.

Historically, the Heti Formation in the Yuanqu Basin yielded the first Eocene vertebrates (including the primate *Hoanghonius stehlinii*) to be discovered in China (*6*). The mammalian fauna from the Heti Formation is usually correlated with the Sharamurunian Land Mammal Age of Asia (*7*) and is therefore probably late middle Eocene in age. The cricetid rodent *Pappocricetodon schaubii* from Locality 1 in the Zhaili Member of the Heti Formation (*8*), the same locality that yielded the eosimiid primate fossils described here, is morphologically more derived than is *P. antiquus*, which occurs in the Shanghuang fissure-fillings (*9*). Indeed, all available biostratigraphic evidence suggests that the new eo-

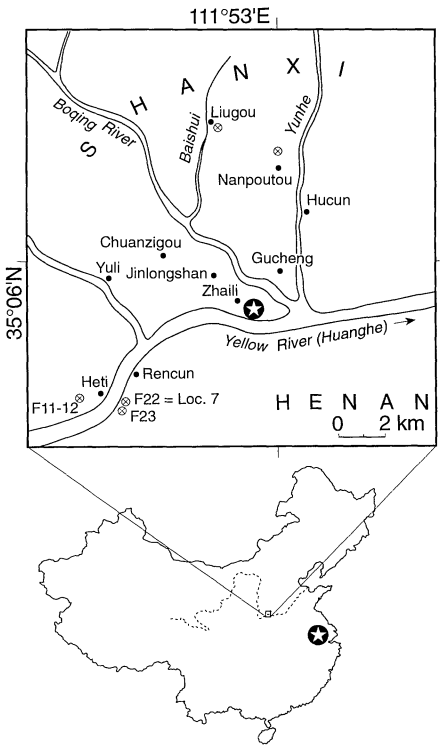

Fig. 1. Map of China with Yellow River drainage (dotted line), showing location of Yuanqu Basin fossil sites (enlargement). Locality 1, the site that yielded the specimens of *E. centennicus* reported here, is represented by a star in the enlargement. The location of the Shanghuang fissure-fillings, provenance of *E. sinensis*, is denoted by a star near the east coast of China.

K. C. Beard and M. R. Dawson, Section of Vertebrate Paleontology, Carnegie Museum of Natural History, 4400 Forbes Avenue, Pittsburgh, PA 15213, USA.
Y. Tong, J. Wang, X. Huang, Institute of Vertebrate Paleontology and Paleoanthropology, Academia Sinica, Post Office Box 643, Beijing, People's Republic of China, 100044.